# A Chiral [2 + 3] Covalent Organic Cage Based on 1,1'-Bi-2-naphthol (BINOL) Units

Midhun Mohan, David-Jérôme Pham, Audrey Fluck, Simon Chapuis, Alain Chaumont, Brice Kauffmann, Laurent Barloy, Pierre Mobian

Chemistry–A European Journal
Communication
doi.org/10.1002/chem.202400458
Chemistry Europe
European Chemical Societies Publishing
www.chemeurj.org

# A Chiral [2+3] Covalent Organic Cage Based on 1,1′-Bi-2-naphthol (BINOL) Units

Midhun Mohan,[a] David-Jérôme Pham,[a] Audrey Fluck,[a] Simon Chapuis,[b] Alain Chaumont,[b] Brice Kauffmann,[c] Laurent Barloy,[a] and Pierre Mobian*[a]

A [2+3] chiral covalent organic cage is produced through a dynamic covalent chemistry approach by mixing two readily available building units, viz. an enantiopure 3,3′-diformyl 2,2′-BINOL compound (**A**) with a triamino spacer (**B**). The two enantiomeric (*R*,*R*,*R*) and (*S*,*S*,*S*) forms of the cage **C** are formed nearly quantitatively thanks to the reversibility of the imine linkage. The X-ray diffraction analysis of cage (*S*,*S*,*S*)-**C** highlights that the six OH functions of the BINOL fragments are positioned inside the cage cavity. Upon reduction of the imine bonds of cage **C**, the amine cage **D** is obtained. The ability of the cage **D** to host the 1-phenylethylammonium cation ($\mathbf{EH}^+$) as a guest is evaluated through UV, CD and DOSY NMR studies. A higher binding constant for (*R*)-$\mathbf{EH}^+$ cation ($Ka = 1.7\ 10^6 \pm 10\%\ M^{-1}$) related to (*S*)-$\mathbf{EH}^+$ ($Ka = 0.9\ 10^6 \pm 10\%\ M^{-1}$) is determined in the presence of the (*R*,*R*,*R*)-**D** cage. This enantiopreference is in close agreement with molecular dynamics simulation.

Shape-persistent organic cages using dynamic covalent imine bonds are intensively investigated, since cages characterized by a large variety of sizes and geometries are accessible from simple building blocks using straightforward synthetic protocols.[1] These fascinating molecular architectures have found many applications including gas sorption,[2] detection of organic pollutants,[3] metal nanoparticles templating[4] or as proton conducting materials.[5] However, chiral versions of organic cages constructed with imine bonds are rare and represent a highly attractive target for chiral molecular recognition.[6] An early example is the one-pot synthesis of a chiral covalent organic [8+12] cage from tris(4-formylphenyl)amine and enantiopure diaminocyclohexane.[7] Another example that relies on a helical building block was obtained by reacting a helicene based dialdehyde with triethylamine as spacer to form a [2+3] cage.[8] Very recently, the use of binaphthyl derivatives has been proposed to generate cages where the source of chirality is provided by the axial chirality originating from the binaphthyl molecular fragments.[9]

2,2′-BINOL (BINOL = 1,1′-bi-2-naphthol) is one of the most popular chiral reagents in chiral technologies.[10] This readily available compound in its enantiopure form (*S* or *R*) shows a high racemization barrier[11] and its derivatization is well documented.[12] Therefore, the 2,2′-BINOL motif looked like an appealing molecular fragment to create chiral organic 3D architectures where the imine linkage is used to assemble the starting building blocks.

Thus, we report the synthesis of a [2+3] imine covalent cage based on an enantiopure 2,2′-BINOL motif. The design of this cage is inspired by the family of cages mainly developed by Mastalerz and co-workers that has in common a salicylimine motif where the imine functions are stabilized by hydrogen bonds completing a six-membered ring and involving a neighboring hydroxyl group.[13]

The 3,3′-diformyl BINOL (**A**) and the triamino spacer (**B**) used to produce the targeted [2+3]-**C** imine cage are depicted in Figure 1. The reaction conditions were optimized and ended to reach a simple and straightforward protocol. The enantiopure compound **A** (*R* or *S*) was mixed with the chloride salt of **B** in the presence of $Et_3N$ in nitrobenzene. The reaction mixture was treated after seven days of reaction at 100 °C by the addition of methanol. The pale-yellow solid that precipitated was isolated and analyzed. Using this synthetic method, the two enantiomeric forms, *i.e.* (*S*,*S*,*S*)-[2+3]-**C** and (*R*,*R*,*R*)-[2+3]-**C**, of the [2+3]-**C** cage were produced almost quantitatively in a multi-hundred-milligram scale (97% yield for (*S*,*S*,*S*)-[2+3]-**C**). Electrospray Ionisation Mass Spectrometry (ESI-MS) analysis displayed two intense peaks at $m/z = 1418.65$ and 709.83 corresponding to $\mathbf{C}+H^+$ and $\mathbf{C}+2H^{2+}$ respectively (calcd for $\mathbf{C}+H^+$, $m/z = 1418.66$; calcd for $\mathbf{C}+2H^{2+}$, $m/z = 709.83$) (see figure S11). $^1$H NMR spectrum of [2+3]-**C** (see figure S7) revealed that the signal of the aldehyde protons of the starting compound **A** was not found any more, while a peak assigned to the imine proton resonance was identified at $\delta = 8.70$ ppm. Furthermore, two doublets integrating for six protons each were observed at $\delta = 4.93$ ppm and $\delta = 4.49$ ppm, corresponding to the $^1$H NMR

[a] Dr. M. Mohan, D.-J. Pham, A. Fluck, Dr. L. Barloy, Dr. P. Mobian
Laboratoire de Synthèse et Fonctions des Architectures Moléculaire (SFAM), UMR 7140 (CMC)
Université de Strasbourg
4, rue Blaise Pascal, CS 90032
67081 Strasbourg Cedex, France
E-mail: mobian@unistra.fr

[b] S. Chapuis, Dr. A. Chaumont
Laboratoire de Modélisation et Simulations Moléculaires, UMR 7140 (CMC)
Université de Strasbourg
4, rue Blaise Pascal, CS 90032
67081 Strasbourg Cedex, France

[c] Dr. B. Kauffmann
Univ. Bordeaux, CNRS, INSERM, IECB, US1, UAR 3033, F-33600 Pessac, France

Supporting information for this article is available on the WWW under https://doi.org/10.1002/chem.202400458

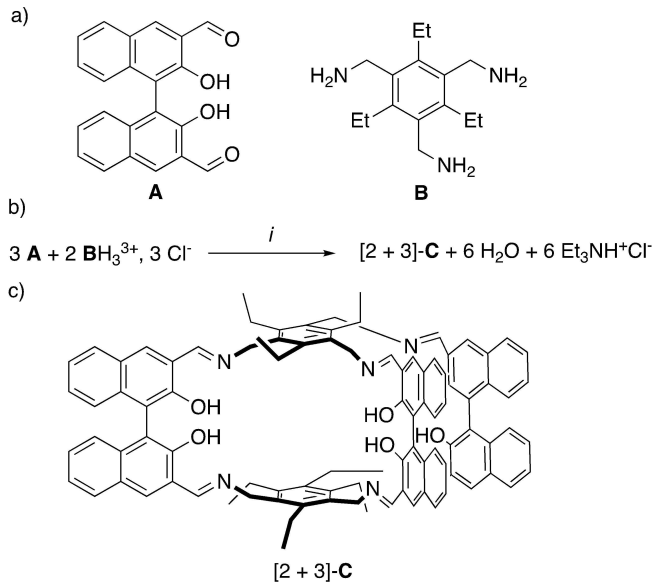


**Figure 1.** a) The 3,3′-diformyl BINOL (**A**) and the triamino spacer (**B**); b) reaction leading to the formation of the [2 + 3] imine cage **C**, reaction conditions: *i*: $Et_3N$, nitrobenzene, 100 °C, 7 days, yield (*S*,*S*,*S*)-[2 + 3]-**C**: 97%, yield (*R*,*R*,*R*)-[2 + 3]-**C**: 96%; c) representation of the imine [2 + 3]-cage **C**.

signature of the diastereotopic $NC\underline{H}_2$ protons. Additionally, Diffusion Ordered Spectroscopy (DOSY) highlighted that compound **C** has a lower diffusion coefficient ($D = 5.87\times10^{-10}$ $m^2.s^{-1}$) than the 2,2′-BINOL derivative **A** ($D = 1.21\times10^{-9}$ $m^2.s^{-1}$) evidencing that the size of the synthetized compound was much larger than the starting building block.

Single crystals of the (*S*,*S*,*S*)-[2 + 3]-**C** cage suitable for X-ray diffraction analysis crystallized directly from the reaction mixture after a few days when methanol vapors were allowed to diffuse in the solution. The crystal contained disordered solvent molecules, which could not be localized, and nitrobenzene molecules interacting strongly with the cage, thus the SQUEEZE command[14] was used to solve the structure by removing the disordered molecules. The compound crystallizes in a triclinic crystal system with a chiral space group (P1). The molecular motif of this cage is shown in Figure 2.

The structure evidences that all the OH groups of the BINOL fragments point inside the cage cavity. The highest distance between two oxygen from two different BINOL fragments is 8.640 Å. The six OH groups of the compound are involved into intramolecular N···HO hydrogen bond interactions with neighboring nitrogen atoms (the N···HO distances are found between 1.827 Å and 1.860 Å and the N···HO angles are measured between 147.57° and 148.69°).

The cage cavity is large enough to host two nitrobenzene molecules. One is hosted in the center of the structure, whereas the other one is stacked between two naphthol units. The close distance of 3.612 Å between the centroid of the nitrobenzene phenyl ring and the centroid of the closest phenyl ring of a naphthol unit attests to π-π interactions. This sheds light on why aromatic solvent permitted to afford the desired cage with an excellent yield whereas the use of non-aromatic solvent such as chlorinated solvents led to undesired products. In order to

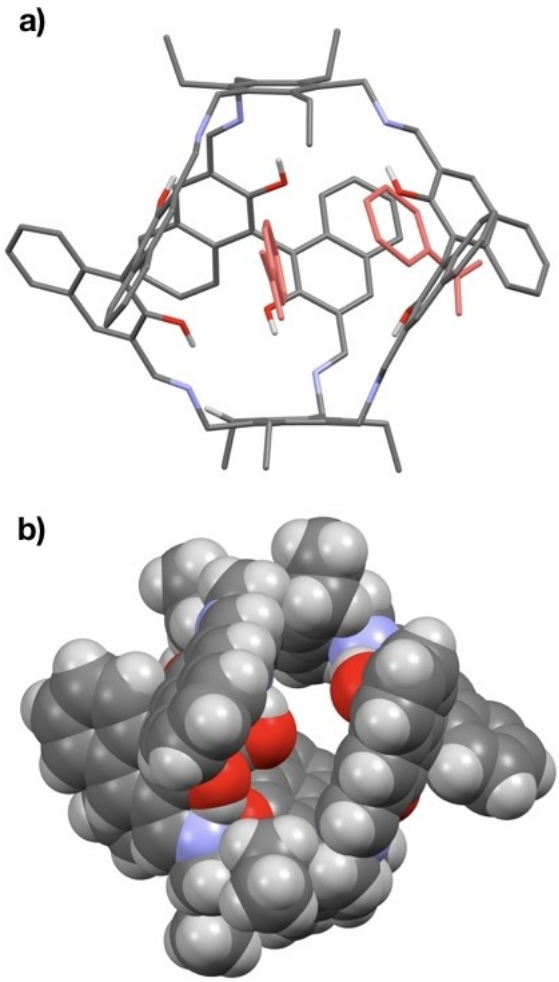


**Figure 2.** Two representations of the molecular structure of the (*S*,*S*,*S*)-[2 + 3]-**C** cage. Carbon atoms are in grey, nitrogen atoms are in blue, oxygen atoms are in red and hydrogen atoms are in light grey. a) The structure of the (*S*,*S*,*S*)-[2 + 3]-**C** cage is viewed with the stick representation. The two co-crystallized nitrobenzene molecules are represented in salmon. Hydrogen atoms are omitted for clarity with the exception of the OH hydrogen evidencing intramolecular N···HO interactions the six OH hydrogen atoms of the structure. b) Spacefill representation of (*S*,*S*,*S*)-[2 + 3]-**C** evidencing the internal cavity of the architecture. For this representation the co-crystallized nitrobenzene molecules have been removed.

determine the available void spaces within the structures of (*S*,*S*,*S*)-**C**, MoloVol calculations based on the crystal structures obtained from XRD were performed.[15] Two-probe mode was employed to specifically analyze the internal cavity of the cage. The difference in the radii of the large and small probe is used to determine the measurements of the inner cavity that are only accessible by the small probe. The small probe with radii of 1.6 Å (comparable to $CO_2$ radii) was employed and the larger probe with the radius of 3 Å. The grid resolution for the calculation was set at 0.2 Å and an optimization depth of 4. The calculations led to values of 463 $Å^3$ for the internal volume of the cage and to 180 $Å^2$ for the accessible internal surface area.

Next, having demonstrated the formation of the targeted cage **C** starting from an enantiopure 3,3′-diformyl BINOL, the chiral self-sorting was evaluated by reacting (*rac*)-(**A**) with **B**. An analysis of the reaction products obtained using the same

synthetic procedure as the one used for the synthesis of the enantiopure cage evidenced no narcissistic self-sorting.[6b] The heterochiral cage isomers (*S*,*S*,*R*)-[2+3]-**C** or (*R*,*R*,*S*)-[2+3]-**C** are predominant *versus* the homochiral cages ((*S*,*S*,*S*)-[2+3]-**C** and (*R*,*R*,*R*)-[2+3]-**C**) and the presence of only [2+3] assemblies was confirmed by ESI-MS analysis showing the $\mathbf{C}+H^+$ and $\mathbf{C}+2H^{2+}$ peaks at *m/z* = 1418.65 and 709.83 respectively. The $^1$H NMR analysis of the reaction products showed two sets of signals (Figure S13). One set corresponded to the homochiral cage isomers ((*S*,*S*,*S*) or (*R*,*R*,*R*) [2+3]-**C**). The other set of peaks corresponded to the heterochiral species, *i.e.* (*R*,*S*,*S*) or (*S*,*R*,*R*). For instance, due to the breaking of symmetry within heterochiral species, the imine protons for the heterochiral cage appeared as three singlets (δ = 8.77, 8.84 and 8.87 ppm). Integrating between the two sets of signals revealed that the proportion of the heterochiral species *versus* the homochiral cage was lower (1.1:1) than the statistical distribution (3:1). This tends to indicate that the homochiral assembly is more stable.

Although the reversibility of imine bonds during the cage formation favors the thermodynamic product, the stability of the cage could be a concern considering the host-guest studies. Reduction of imine bonds to amine linkages was performed to improve the cage stability.[9a] This is achieved by reduction of (*S*,*S*,*S*)-**C** or (*R*,*R*,*R*)-**C** using $NaBH(OAc)_3$ in $CHCl_3$ forming (*S*,*S*,*S*)-**D** or (*R*,*R*,*R*)-**D** (Figure 3) respectively in around 60% yield. After reduction, by $^1$H NMR, the imine proton signal at δ = 8.62 ppm has disappeared and two complex signals are now observed at δ = 4.20 and 3.74 ppm for the $NHC\underline{H}_2$ protons (Figure S9). Single crystals of the (*S*,*S*,*S*)-[2+3]-**D** cage suitable for X-ray diffraction analysis were obtained by slow diffusion of acetonitrile into a solution of the cage in dichloromethane. The molecular structure is given in Figure S14. As attested by the analysis of the crystal structure, the reduction induces a slight modification of the internal volume of the cage. Here, the highest oxygen-oxygen distance is 9.4 Å, representing an increase of 9% of the O···O distance related to the imine cage. The accessible internal surface area and the internal volume were calculated using the MoloVol software at 125 $Å^2$ and 328 $Å^3$ respectively for the amine cage **D**. These values reflect a smaller internal volume related to the imine cage linked to an increase of flexibility after the imine bond reduction. Concerning the optical properties, in the UV-visible spectra of the cages, the imine cage absorbs light in the visible domain, whereas the amine compound displays optical properties only in the UV region, revealing a higher conjugation for the cage **C** compared to **D** (Figure S18). A marked difference concerning the chiroptical properties between **D** and **C** is also found. The circular dichroism spectra of the two enantiomeric forms of cages **C**, **D** and the BINOL derivative **A** are compiled in Figure S21. Interestingly, the CD spectra of cage **C** and compound **A** having the same stereochemical descriptor are similar with two notable exceptions: one concerning the intensity (the CD spectrum of **C** is roughly three times more intense) and the second linked to the presence of a circular dichroism signal above 300 nm for **C**. Overall, for two cages having the same stereochemical descriptors, the CD spectrum of **D** is hypsochromically-shifted compared to the spectrum of **C**.

Initially, several potential chiral and achiral guests (see Table S26) were selected to interact with the imine cage **C** but no host-guest interactions were observed. Nevertheless, the formation of a complex with the ammonium cation $\mathbf{E}H^+$ (Figure 4) and cage **D** was highlighted. This compound, $\mathbf{E}H^+$, was selected due to a previously reported naphthol-based cage showing high binding affinities for different monocharged organic cations.[16] Therefore, the *R* and *S* enantiomers of 1-phenyl-ethyl-ammonium cation ($\mathbf{E}H^+$) associated with the tetrakis 3,5-bis(trifluoromethyl)phenyl borate anion ($BARF^-$) were mixed with an enantiopure amine cage **D**.[17] These experiments were monitored by $^1$H NMR, circular dichroism and UV-visible spectroscopy. Firstly, for the host-guest experiments conducted with the enantiopure amine **E** in the presence of one enantiomer of the cage **D**, no specific interaction between the cage and the amine was evidenced. By contrast, significant shifts of several sharp resonances of the $^1$H-NMR spectrum of (*R*,*R*,*R*)-**D** were observed upon adding one equivalent of the

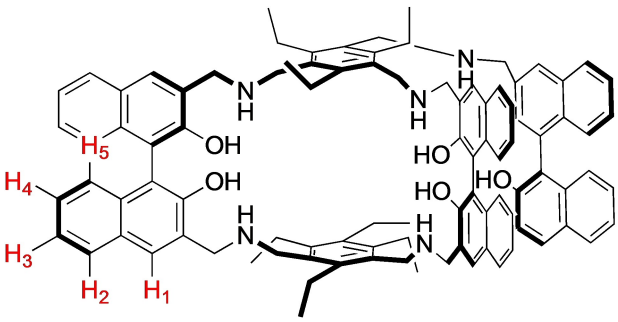


**Figure 3.** Representation of the amine cage (*R*,*R*,*R*)-**D** with labelled aromatic protons.

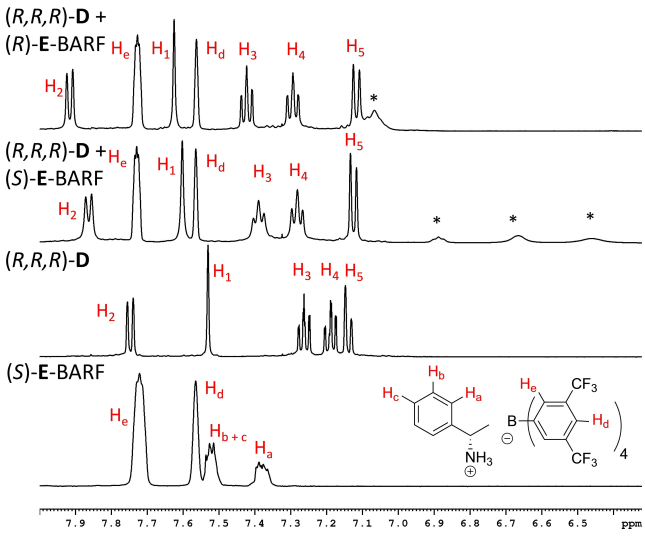


**Figure 4.** Aromatic region from 6.3 ppm to 8 ppm of the $^1$H NMR spectra of the enantiopure cage **D** associated with one equivalent of the (*S*) or the (*R*) form of the ammonium cation $\mathbf{E}H^+$ (500 MHz, $CD_2Cl_2$). For comparison, the spectra of the cage **D** (500 MHz, $CD_2Cl_2$) and the **E**H-BARF (300 MHz, $CD_2Cl_2$) are given. The signals labelled with the stars correspond to the ammonium cation hosted by the cage.

enantiopure ammonium chiral salt ((*S*)-**E**H-BARF and (*R*)-**E**H-BARF), (see Figure 4). The chemical shift changes for each proton resonance of the cage ($\Delta\delta$), that were different depending on the *R* or *S* enantiomer of $\mathbf{E}H^+$ added to the cage, are compiled in Table S17. It is also important to note that with two equivalents of the chiral salt the $^1$H NMR spectrum looked very similar to the one recorded with one equivalent. A control experiment with the addition of HCl (one equivalent) was conducted where the $^1$H NMR spectrum of (*R*,*R*,*R*)-**D** underwent no modification, implying that the chemical shift changes did not originate from protonation of the cage. Concerning the NMR signature of the salt in the presence of the cage, the signals of the BARF anion were identical as those observed for the free salt whereas the signals of the ammonium cation appeared very broad and strongly shielded compared to the free salt (all these protons resonate below 7.1 ppm) (see Figure 4 and Figure S21 and S22 at 298 K). The broadening of the signals corresponding to the ammonium arose from a dynamic phenomenon, as drastic modification of these large signals was observed when the sample was cooled to 203 K. However, no coalescence was noticed in the range of temperature used. The DOSY 2D map of the host-guest experiment at room temperature indicated a diffusion coefficient for $\mathbf{E}H^+$ that is similar with the diffusion coefficient measured for $\mathbf{E}H^+$ without the cage at room temperature (Figure S23). The situation changed drastically when the NMR DOSY experiment was recorded at 203 K (see Figure S25 and Figure 5). In this case, two species were present in solution. The diffusion at $D = 7.8\times10^{-11}$ m$^2$.s$^{-1}$ measured for the larger species is much lower in comparison with the diffusion evaluated for the BARF anion ($D = 1.00\times10^{-10}$ m$^2$.s$^{-1}$). Importantly, this diffusion was assigned to the signals belonging to cage **D** and the ammonium cation highlighting the formation of a (*S*)-$\mathbf{E}H^+\subset$(*R*,*R*,*R*)-**D** host-guest system stable at low temperature on the NMR time-scale.

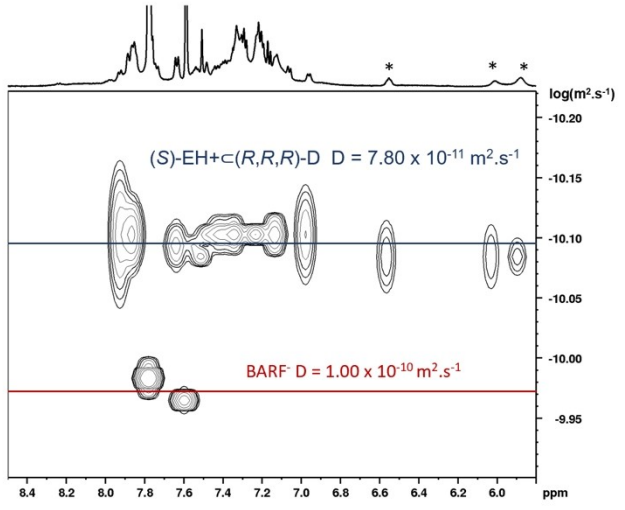


**Figure 5.** Low temperature DOSY NMR (5.8–8.45 ppm) of (*R*,*R*,*R*)-**D** + (*S*)-**E**H-BARF (proton resonances marked with the stars correspond to the ammonium proton signals) (1 : 1) recorded at 203 K (600 MHz, $CD_2Cl_2$).

Complexation of **E**H-BARF by the cage in solution was investigated more in details with UV-visible and circular dichroism spectroscopy to characterize the host-guest interaction. Upon a gradual addition of the enantiopure **E**H-BARF into a stock solution of the (*R*,*R*,*R*)-**D** in dichloromethane, the circular dichroism spectra showed several modifications in the region between 220 and 250 nm similar for both enantiomers of the cation with a plateau reached upon the addition of one equivalent of **E**H-BARF (Figure S28–29). It should be noted that in this region, both enantiomers of the **E**H-BARF salt are CD silent. UV-visible titration of (*R*,*R*,*R*)-**D** with (*S*)- or (*R*)-**E**H-BARF was performed in DCM to evaluate the strength of the interaction (Figure S31). Data were fitted to a 1 : 1 stoichiometry and gave a binding constant $K_a = 0.9\ 10^6 \pm 10\%\ M^{-1}$ and $K_a = 1.7\ 10^6 \pm 10\%\ M^{-1}$ for (*S*)-**E**H-BARF or (*R*)-**E**H-BARF respectively showing that the (*R*)-$\mathbf{E}H^+$ cation bound more strongly the cage *versus* the (*S*)-$\mathbf{E}H^+$ enantiomer (Figure S33).[18]

Further insights on the microscopical level of the previous investigated systems have been obtained via classical molecular dynamics (cMD). (See SI for Methodological details). At first 2 cMD trajectories of 2.5 μs each have been obtained for the systems composed of an equimolecular ratio of the (*R*,*R*,*R*)-**D** cage and either (*S*)-**E** or (*R*)-**E** amine in DCM. During these simulations the (*S*)-**E** or (*R*)-**E** amine are found at an average distance of about 30.0 ± 8.0 Å from the centre of mass (CoM) of the (*R*,*R*,*R*)-**D** cage showing no strong interactions between the (*R*,*R*,*R*)-**D** cage and the amine molecules (Figure S35). Furthermore, calculated interaction energies, averaged over the whole trajectory, between (*R*,*R*,*R*)-**D** cage and either the (*R*)-**E** (−0.1 ± 0.6 kcal/mol) or (*S*)-**E** amine (−0.2 ± 1.4 kcal/mol), confirm the lack of interaction between the (*R*,*R*,*R*)-**D** cage and both amines. This may result from the fact that inside the cavity of the (*R*,*R*,*R*)-**D** cage two DCM molecules can be found (Figure S36) interacting via hydrogen bonds with the (*R*,*R*,*R*)-**D** cage, and interactions between the amines and the (*R*,*R*,*R*)-**D** cage may not be sufficiently strong to chase the molecules outside of (*R*,*R*,*R*)-**D**. In a second step two further molecular dynamics simulations of 10 μs were computed, each containing an equimolar ratio of either (*S*)-**E**H-BARF or (*R*)-**E**H-BARF and (*R*,*R*,*R*)-**D** cage. During both simulations, we observe the capture of the ammonium cation by the (*R*,*R*,*R*)-**D** cage. While the complexation of the (*S*)-$\mathbf{E}H^+$ cation is seen to take place after about 30 ns, complexation of the (*R*)-$\mathbf{E}H^+$ is found to happen after 15 ns, indicating that there is only a small to no energy barrier for it to enter the (*R*,*R*,*R*)-**D** cage. Once these complexes are formed, they were found to remain stable during the rest of the remaining dynamics (Figure S36). Radial distribution functions (RDF) of the CoM of the ammonium cation around the CoM of the (*R*,*R*,*R*)-**D** cage (Figure 6) point to the fact that the position, and the dynamics, of both ammonium cations inside the cavity differ. While the (*R*)-$\mathbf{E}H^+$ ammonium cation fits nicely inside the cavity of the (*R*,*R*,*R*)-**D** cage remaining throughout the dynamics at an average distance of 0.7 Å from the CoM of the (*R*,*R*,*R*)-**D** cage, the (*S*)-$\mathbf{E}H^+$ cation is found to jiggle between two distinct positions within the (*R*,*R*,*R*)-**D** cage, with a first conformation at a distance of about 1.0 Å from the centre of the cavity and a second conformation at about 2.6–2.7 Å (Figure 6). Insights into

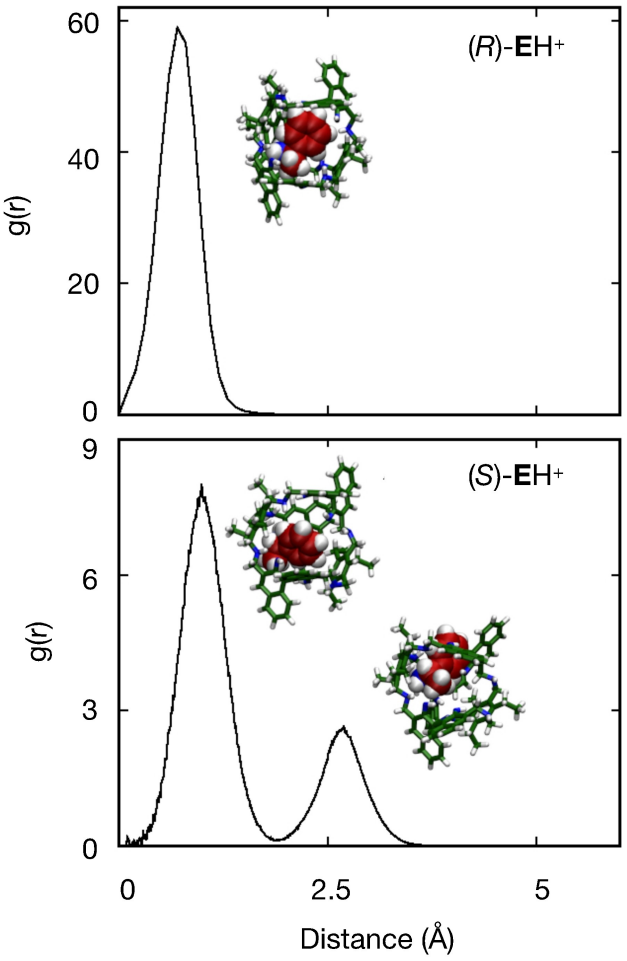


**Figure 6.** Radial distribution function of the Centre of Mass of the (*R*)-**E**H$^+$ or (S)-**E**H$^+$ around the center of the *(R,R,R)*-**D** cage and representative structures of the complex structures corresponding to the various maxima of the RDFs.

the energetics reveal that the interaction energies between the (*R*,*R*,*R*)-**D** cage and either the (*R*)-**E**H$^+$ or the (*S*)-**E**H$^+$ are found to be identical ($-83.2 \pm 5.1$ kcal.mol$^{-1}$ and $-83.2 \pm 6.8$ kcal.mol$^{-1}$, respectively). However, solvation energy of the (*R*,*R*,*R*)-**D** cage is found to be larger in the case of the (*R*)-**E**H$^+$ complex ($-164.8 \pm 8.3$ kcal.mol$^{-1}$) than in the system containing (*S*)-**E**H$^+$ ($-157.5 \pm 10.5$ kcal.mol$^{-1}$), while on the other hand the (*S*)-**E**H$^+$ ammonium cation is to be better solvated ($-31.2 \pm 7.4$ kcal.mol$^{-1}$) than the (*R*)-**E**H$^+$ ammonium cation ($-26.7 \pm 7.0$ kcal.mol$^{-1}$). Overall this showns that the (*R*)-**E**H$^+$⊂(*R*,*R*,*R*)-**D** is slightly better solvated by about 2.8 kcal.mol$^{-1}$ than its (*S*)-**E**H$^+$ ⊂(*R*,*R*,*R*)-**D** counterpart ($-191.5$ vs. $-188.7$ kcal.mol$^{-1}$, respectively), pointing to the fact that the selectivity of the (*R*,*R*,*R*)-**D** cage results from solvation effects. To further investigate the selectivity of the (*R*,*R*,*R*)-**D** host we performed thermodynamic integration calculations. The obtained results reveal a $\Delta G_{Comp}$ in the case of the (*R*)-**E**H$^+$ ammonium cation of about $-29.0$ kcal.mol$^{-1}$ and about $-26.7$ kcal.mol$^{-1}$ in the case of the (*S*)-**E**H$^+$ ammonium cation (Figure S38). The difference in free energy ($\Delta\Delta G_{Comp}$) is about 2.3 kcal.mol$^{-1}$ in favour of the (*R*)-**E**H$^+$ ammonium cation confirming the experimental results.

In summary, the efficient formation of an enantiopure [2 + 3]-cage based on imine bonds starting from readily accessible building blocks was reported. The X-ray diffraction analysis attested the formation of the desired assembly where the OH functions of the BINOL moieties are located inside the cavity of the architecture. The imine cage was converted into the stable cage **D** by using $NaBH(OAc)_3$ as a reducing agent. The reduction impacts the morphology of the cage in the crystalline solid-state. The presence of a large cavity allowed the interaction with a guest. The host-guest complex formation was evidenced by mixing in solution the cage (*R*,*R*,*R*)-**D** with enantiopure cations **E**H$^+$ associated with the BARF counter-anion. Low temperature DOSY NMR analysis proved the generation of the **E**H$^+$⊂(*R*,*R*,*R*)-**D** association whereas the amine **E** did not interact with the cage. Remarkably, a preference of the (*R*,*R*,*R*)-**D** cage to host the *R* enantiomer of **E**H$^+$ related to (*S*)-**E**H$^+$ was evidenced through the determination of the binding constants. This host-guest enantioselectivity was supported by molecular dynamic simulations. Whereas the chiral organic cages built from the 2,2′-BINOL fragment reported until now concerned mostly BINOL protected cages,[9] the cages **D** or **C** contains six OH groups decorating the internal environment of the 3D architecture which opens fascinating opportunities in chiral technologies, molecular recognition or coordination chemistry.

## Acknowledgements

We thank the USIAS (Institut d'études avancées de l'Université de Strasbourg), the University of Strasbourg and the CNRS for financial support. Dr. M. Mohan thanks the USIAS for his post-doctoral fellowship. In the framework of the CNRS ЯÉCIPROCS network, this work has benefited from the X-ray facility of the Biophysical and Structural Chemistry platform at IECB, CNRS UMS3033, INSERM US001, Bordeaux University. Also, we owe a debt of gratitude to Dr. Jean-Claude Chambron for fruitful discussions. For the purpose of Open Access, a CC-BY public copyright licence has been applied by the authors to the present document and will be applied to all subsequent versions up to the Author Accepted Manuscript arising from this submission.

## Conflict of Interests

The authors declare no conflict of interest.

## Data Availability Statement

The data that support the findings of this study are available in the supplementary material of this article.

**Keywords:** Chirality · Organic cage · BINOL · host-guest

[1] a) For a general review on covalent cage see: G. Montà-González, F. Sancenón, R. Martínez-Máñez, V. Martí-Centelles, *Chem. Rev.* **2022**, *122* (16), 13636; For a review dedicated on imine covalent cage exclusively see: b) K. Acharyya, P. S. Mukherjee, *Angew. Chem. Int. Ed.* **2019**, *58*, 8640; c) X. Liu, Y. Liu, G. Li, R. Warmuth, *Angew. Chem. Int. Ed.* **2006**, *45*, 901; for for metal-based assemblies formed with imine linkage see: d) T. K. Ronson, S. Zarra, S. P. Black, J. R. Nitschke, *Chem. Commun.* **2013**, *49*, 2476.

[2] a) K. Qu, J. Xu, L. Dai, Y. Wang, H. Cao, D. Zhang, Y. Wu, W. Xu, K. Huang, C. Lian, X. Guo, W. Jin, Zhi Xu, *Angew. Chem. Int. Ed.* **2022**, *61*(31), e202205481; b) K. Jie, N. Onishi, J. A. Schott, I. Popovs, D. E. Jiang, S. Mahurin, S. Dai, *Angew. Chem. Int. Ed.* **2020**, *59*, 2268; *Angew. Chem.* **2020**, *132*, 2288; c) M. Liu, L. Chen, S. Lewis, S. Y. Chong, M. A. Little, T. Hasell, I. M. Aldous, C. M. Brown, M. W. Smith, C. A. Morrison, L. J. Hardwick, A. I. Cooper, *Nat. Commun.* **2016**, *7*, 12750; d) M. Liu, M. A. Little, K. E. Jelfs, J. T. A. Jones, M. Schmidtmann, S. Y. Chong, T. Hasell, A. I. Cooper, *J. Am. Chem. Soc.* **2014**, *136*, 7583; e) Q. Song, S. Jiang, T. Hasell, M. Liu, S. Sun, A. K. Cheetham, E. Sivaniah, A. I. Cooper, *Adv. Mater.* **2016**, *28*, 2629; f) T. Hasell, S. Y. Chong, K. E. Jelfs, D. J. Adams, A. I. Cooper, *J. Am. Chem. Soc.* **2012**, *134*, 588.

[3] a) K. Acharyya, A. Chowdhury, B. Mondal, S. Chakraborty, P. S. Mukherjee, *Chem. Eur. J.* **2017**, *23*, 8482; b) M. A. Zwijnenburg, E. Berardo, W. J. Peveler, K. E. Jelfs, *J. Phys. Chem. B* **2016**, *120*, 5063; c) K. Acharyya, P. S. Mukherjee, *Chem. Eur. J.* **2015**, *21*, 6823; d) K. Acharyya, P. S. Mukherjee, *Chem. Commun.* **2014**, *50*, 15788; e) M. Brutschy, M. W. Schneider, M. Mastalerz, S. R. Waldvogel, *Chem. Commun.* **2013**, *49*, 8398; f) M. Brutschy, M. W. Schneider, M. Mastalerz, S. R. Waldvogel, *Adv. Mater.* **2012**, *24*, 6049.

[4] a) L. Qiu, R. McCaffrey, Y. Jin, Y. Gong, Y. Hu, H. Sun, W. Park, W. Zhang, *Chem. Sci.* **2018**, *9*, 676; b) Y. Zhang, Y. Xiong, J. Ge, R. Lin, C. Chen, Q. Peng, D. Wang, Y. Li, *Chem. Commun.* **2018**, *54*, 2796; c) B. Mondal, K. Acharyya, P. Howlader, P. S. Mukherjee, *J. Am. Chem. Soc.* **2016**, *138*, 1709; d) J. K. Sun, W. W. Zhan, T. Akita, Q. Xu, *J. Am. Chem. Soc.* **2015**, *137*, 7063; e) R. McCaffrey, H. Long, Y. Jin, A. Sanders, W. Park, W. Zhang, *J. Am. Chem. Soc.* **2014**, *136*, 1782.

[5] M. Liu, L. Chen, S. Lewis, S. Y. Chong, M. A. Little, T. Hasell, I. M. Aldous, C. M. Brown, M. W. Smith, C. A. Morrison, L. J. Hardwick, A. I. Cooper, *Nat. Commun.* **2016**, *7*, 12750.

[6] a) For a general review see: F. Begato, G. Licini, C. Zonta, *Angew. Chem. Int. Ed.* **2023**, *62* (51), e202311153; b) F. Esteve, B. Altava, E. Garcia-Verdugo, S. V. Luis, J.-M. Lehn, *Chem.* **2022**, *8*, 2023 ; c) M. Wierzbicki, A. A. Głowacka, M. P. Szymańskia, A. Szumna, *Chem. Commun.* **2017**, *53*, 5200; d) Y.-L. Sun, Z. Wang, H. Ma, Q.-P. Zhang, B.-B. Yang, X. Meng, Y. Zhang, C. Zhang, *Chem. Commun.* **2023**, *59*, 302.

[7] K. E. Jelfs, X. Wu, M. Schimdtmann, J. T. A. Jones, J. E. Warren, D. J. Adams, A. I. Cooper, *Angew. Chem. Int. Ed.* **2011**, *50*, 10653.

[8] A. U. Malik, F. Gan, C. Shen, N. Yu, R. Wang, J. Crassous, M. Shu, H. Qiu, *J. Am. Chem. Soc.* **2018**, *140*, 2769.

[9] a) E. Ramakrishna, J.-D. Tang, J.-J. Tao, Q. Fang, Z. Zhang, J. Huang, S. Li, *Chem. Commun.* **2021**, *57*, 9088; b) D.-X. Cui, Y. Geng, J.-N. Kou, G.-G. Shan, C.-Y. Sun, K.-H. Zhang, X.-L. Wang, Z.-M. Su, *Nat. Commun.* **2022**, *13*, 4011.

[10] J. M. Brunel, *Chem. Rev.* **2005**, *105(3)*, 857.

[11] L. Meca, D. Řeha, Z. Havlas, *J. Org. Chem.* **2003**, *68(14)*, 5677.

[12] Y. Chen, S. Yekta, A. K. Yudin, *Chem. Rev.* **2003**, *103*, 3155.

[13] a) P. Wagner, F. Rominger, J. H. Gross, M. Mastalerz, *Angew. Chem. Int. Ed.* **2023**, *62*, e202217251; b) B. P. Benke, T. Kirschbaum, J. Graf, J. H. Gross, M. Mastalerz, *Nat. Chem.* **2023**, *15*, 413; c) F. Uhrmacher, S. M. Elbert, F. Rominger, M. Mastalerz, *Eur. J. Inorg. Chem.* **2022**, e202100864; d) M. Holsten, S. Feierabend, S. M. Elbert, F. Rominger, T. Oeser, M. Mastalerz, *Chem. Eur. J.* **2021**, *27*, 9383; e) P. Wagner, F. Rominger, W.-S. Zhang, J. H. Gross, S. M. Elbert, R. R. Schröder, M. Mastalerz, *Angew. Chem. Int. Ed.* **2021**, *60*, 8896; f) Michael Mastalerz, *Acc. Chem. Res.* **2018**, *51*, 2411; g) D. Beaudoin, F. Rominger, M. Mastalerz, *Angew. Chem. Int. Ed.* **2017**, *56* 1244.

[14] A. L. Spek, *Acta Crystallogr. Sect. C* **2015**, *71*, 9.

[15] J. B. Maglic, R. Lavendomme, *J. Appl. Crystallogr.* **2022**, *55(4)*, 1033.

[16] F. Jia, H. Hupatz, L. P. Yang, H. V. Schröder, D. H. Li, S. Xin, D. Lentz, F. Witte, X. Xie, B. Paulus, C. A. Schalley, W. Jiang, *J. Am. Chem. Soc.* **2019**, *141*, 4468.

[17] An initial experiment was performed with the hexafluorophosphate salt of $\mathbf{E}H^+$ ($\mathbf{E}HPF_6$) in the presence of the imine cage **C**. The $\mathbf{E}H$-$PF_6$ salt was unstable due to the decomposition of the $PF_6^-$ anion according to $^{19}F$ NMR analysis. Also, when cage **C** was mixed with $\mathbf{E}H$-$PF_6$, ESI-MS and DOSY analysis indicated that the cage has partially collapsed to form 3,3′-bis-((1-phenylethyl)imino)methyl)-1,1′-binaphthtol as a major product (see Figure S32). However, by ESI-MS, a peak at $m/z = 1538.75$ (calcd for $\mathbf{E}H \subset \mathbf{C}$; $m/z = 1538.74$) was detected demonstrating the presence of the host-guest system in solution.

[18] P. Thordarson, *Chem. Soc. Rev.* **2011**, *40*, 1305.

Manuscript received: February 1, 2024
Accepted manuscript online: March 1, 2024
Version of record online: ■■, ■■

# COMMUNICATION

A chiral cage formed with three 2,2′-BINOL units was prepared through a dynamic covalent chemistry approach. This architecture contains six OH functions pointing inside the cavity. Host-guest studies demonstrated enantiopreference of the cage for a chiral ammonium cation.

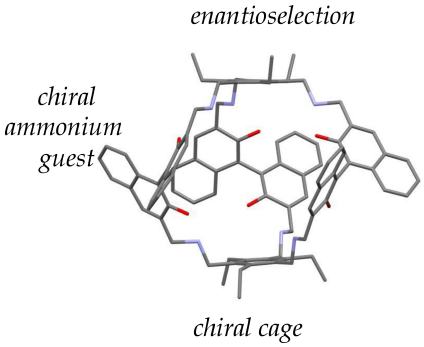


*Dr. M. Mohan, D.-J. Pham, A. Fluck, S. Chapuis, Dr. A. Chaumont, Dr. B. Kauffmann, Dr. L. Barloy, Dr. P. Mobian**

1 – 7

**A Chiral [2+3] Covalent Organic Cage Based on 1,1′-Bi-2-naphthol (BINOL) Units**